should be a more generic phenomenon relevant to other intermetallic compounds.

Note added in proof: While this paper was being reviewed, J. Buhot *et al.* (*32*) reproduced the A_{2g} symmetry in-gap mode in a Raman experiment with 561-nm laser excitation and showed that the mode does not split in up to 10 T magnetic field.

REFERENCES AND NOTES

1. G. R. Stewart, *Rev. Mod. Phys.* **56**, 755–787 (1984).
2. P. Santini *et al.*, *Rev. Mod. Phys.* **81**, 807–863 (2009).
3. T. T. M. Palstra *et al.*, *Phys. Rev. Lett.* **55**, 2727–2730 (1985).
4. M. B. Maple *et al.*, *Phys. Rev. Lett.* **56**, 185–188 (1986).
5. P. Santini, G. Amoretti, *Phys. Rev. Lett.* **73**, 1027–1030 (1994).
6. K. Haule, G. Kotliar, *Nat. Phys.* **5**, 796–799 (2009).
7. S. Elgazzar, J. Rusz, M. Amft, P. M. Oppeneer, J. A. Mydosh, *Nat. Mater.* **8**, 337–341 (2009).
8. P. Chandra, P. Coleman, J. A. Mydosh, V. Tripathi, *Nature* **417**, 831–834 (2002).
9. H. Ikeda *et al.*, *Nat. Phys.* **8**, 528–533 (2012).
10. P. Chandra, P. Coleman, R. Flint, *Nature* **493**, 621–626 (2013).
11. J. A. Mydosh, P. M. Oppeneer, *Rev. Mod. Phys.* **83**, 1301–1322 (2011) and references therein.
12. D. A. Bonn, J. D. Garrett, T. Timusk, *Phys. Rev. Lett.* **61**, 1305–1308 (1988).
13. C. Broholm *et al.*, *Phys. Rev. B* **43**, 12809–12822 (1991).
14. C. R. Wiebe *et al.*, *Nat. Phys.* **3**, 96–99 (2007).
15. P. Aynajian *et al.*, *Proc. Natl. Acad. Sci. U.S.A.* **107**, 10383–10388 (2010).
16. F. Bourdarot *et al.*, *J. Phys. Soc. Jpn.* **79**, 064719 (2010).
17. J. S. Hall *et al.*, *Phys. Rev. B* **86**, 035132 (2012).
18. W. T. Guo *et al.*, *Phys. Rev. B* **85**, 195105 (2012).
19. R. Okazaki *et al.*, *Science* **331**, 439–442 (2011).
20. S. Tonegawa *et al.*, *Nat. Commun.* **5**, 4188 (2014).
21. J. R. Jeffries, K. T. Moore, N. P. Butch, M. B. Maple, *Phys. Rev. B* **82**, 033103 (2010).
22. See supplementary materials on *Science* Online.
23. L. N. Ovander, *Opt. Spectrosc.* **9**, 302 (1960).
24. J. A. Koningstein, O. S. Mortensen, *Nature* **217**, 445–446 (1968).
25. S. L. Cooper, M. V. Klein, M. B. Maple, M. S. Torikachvili, *Phys. Rev. B* **36**, 5743–5746 (1987).
26. B. S. Shastry, B. I. Shraiman, *Int. J. Mod. Phys. B* **5**, 365–388 (1991).
27. D. V. Khveshchenko, P. B. Wiegmann, *Phys. Rev. Lett.* **73**, 500–503 (1994).
28. H. Rho, M. V. Klein, P. C. Canfield, *Phys. Rev. B* **69**, 144420 (2004).
29. F. Bourdarot, B. Fåk, K. Habicht, K. Prokeš, *Phys. Rev. Lett.* **90**, 067203 (2003).
30. C. Bareille *et al.*, *Nat. Commun.* **5**, 4326 (2014).
31. A. R. Schmidt *et al.*, *Nature* **465**, 570–576 (2010).
32. J. Buhot *et al.*, *Phys. Rev. Lett.* **113**, 266405 (2014).

ACKNOWLEDGMENTS

We thank J. Buhot, P. Chandra, P. Coleman, G. Kotliar, M.-A. Méasson, D. K. Morr, L. Pascut, A. Sacuto, J. Thompson, and V. M. Yakovenko for discussions. G.B. and V.K.T. acknowledge support from the U.S. Department of Energy, Office of Basic Energy Sciences, Division of Materials Sciences and Engineering under Award DE-SC0005463. H.-H.K. acknowledges support from the National Science Foundation under Award NSF DMR-1104884. K.H. acknowledges support by NSF DMR-1405303. W.-L.Z. acknowledges support by the Institute for Complex Adaptive Matter (NSF-IMI grant DMR-0844115). Work at Los Alamos National Laboratory was performed under the auspices of the U.S. Department of Energy, Office of Basic Energy Sciences, Division of Materials Sciences and Engineering.

SUPPLEMENTARY MATERIALS

www.sciencemag.org/content/347/6228/1339/suppl/DC1
Material and Methods
Figs. S1 to S4
References (*33*–*46*)

3 March 2014; accepted 30 January 2015
Published online 12 February 2015;
10.1126/science.1259729

APPLIED OPTICS

Multiwavelength achromatic metasurfaces by dispersive phase compensation

Francesco Aieta,* Mikhail A. Kats,† Patrice Genevet,‡ Federico Capasso§

The replacement of bulk refractive optical elements with diffractive planar components enables the miniaturization of optical systems. However, diffractive optics suffers from large chromatic aberrations due to the dispersion of the phase accumulated by light during propagation. We show that this limitation can be overcome with an engineered wavelength-dependent phase shift imparted by a metasurface, and we demonstrate a design that deflects three wavelengths by the same angle. A planar lens without chromatic aberrations at three wavelengths is also presented. Our designs are based on low-loss dielectric resonators, which introduce a dense spectrum of optical modes to enable dispersive phase compensation. The suppression of chromatic aberrations in metasurface-based planar photonics will find applications in lightweight collimators for displays, as well as chromatically corrected imaging systems.

Refractive and diffractive optical components have fundamentally different responses to broadband light. For a material with normal dispersion, refractive lenses have larger focal distances for red light than for blue and prisms deflect longer wavelengths by a smaller angle; the contrary occurs for diffractive lenses and gratings (*1*, *2*). This contrasting behavior arises because two different principles are used to shape the light: Refractive optics relies on the phase gradually accumulated through propagation, whereas diffractive optics operates by means of interference of light transmitted through an amplitude or phase mask. In most transparent materials in the visible, the refractive index n decreases with increasing wavelength (λ) (normal dispersion). Because the deflection angle θ of a prism increases with n and a lens focal length f is inversely proportional to $n - 1$, the resulting effect is the one shown in Fig. 1, A and B. In a diffractive optical element (DOE), the beam deflection angle and the focal length instead increase and decrease with λ, respectively (Fig. 1, C and D), generating an opposite dispersion compared with standard refractive devices. Although for many applications a spatial separation of different wavelengths is desirable, in many others this represents a problem. For example, the dependence of the focal distance on λ produces chromatic aberrations and is responsible for the degradation of the quality of an imaging system. Another difference between these technologies is the efficiency that is generally lower for diffractive optics due to the presence of higher diffraction orders. The wavelength dependence is typically much more pronounced in diffractive optics than in refractive optics, when low-dispersion materials are used in the latter (*2*). In refractive lenses, complete elimination of chromatic aberrations at two and three wavelengths is accomplished using, respectively, two and three elements (achromatic doublet and apochromatic triplet) arranged to achieve the same focal length at the wavelengths of interest (*3*). Superachromatic lenses are practically achromatic for all colors by correcting aberrations at four suitable wavelengths (*4*). Although successful, these strategies add weight, complexity, and cost to optical systems. On the other hand, DOEs have the advantage of being relatively flat, light, and often low cost. Blazed gratings and Fresnel lenses are diffractive optical devices with an analog phase profile and integrate some benefits of both technologies (e.g., small footprint and high efficiency), but they still suffer from strong chromatic aberrations. Multiorder diffractive lenses overcome this limitation by using thicker phase profiles to achieve chromatic correction for a discrete set of wavelengths (*1*). However, the realization of thick, analog phase profiles is challenging for conventional fabrication technologies.

Metasurfaces are thin optical components that rely on a different approach for light control: A dense arrangement of subwavelength resonators is designed to modify the optical response of the interface. The resonant nature of the scatterers introduces an abrupt phase shift in the incident wavefront, making it possible to mold the scattered wavefront at will and enabling a new class of planar photonics components (flat optics) (*5*–*8*). Different types of resonators (metallic or dielectric antennas, apertures, etc.) have been used to demonstrate various flat optical devices, including blazed gratings (*9*–*11*), lenses (*12*–*14*), holographic plates (*15*), polarizers, and wave plates

School of Engineering and Applied Sciences, Harvard University, Cambridge, MA 02138, USA.
*Present address: Hewlett-Packard Laboratories, Palo Alto, CA 94304, USA. †Present address: Department of Electrical and Computer Engineering, University of Wisconsin, Madison, WI 53706, USA. ‡Present address: Singapore Institute of Manufacturing Technology (SIMTech), Singapore 638075, Singapore. **§Corresponding author. E-mail: capasso@seas.harvard.edu**

(*6*, *16*). The metasurface approach is distinct in that it provides continuous control of the phase profile (i.e., from 0 to 2π) with a binary structure (only two levels of thickness), circumventing the fundamental limitation of multiple diffraction orders while maintaining the size, weight, and ease-of-fabrication advantages of planar diffractive optics (*5*–*8*). However, the metasurface-based optical devices demonstrated so far are affected by large chromatic aberrations, though research efforts have shown that relatively broadband optical metasurfaces can be achieved (*6*, *10*, *11*, *13*–*15*). This claim of large bandwidth refers to the broadband response of the resonators, which is the result of the high radiation losses necessary for high scattering efficiency and, to a lesser extent, of the absorption losses (*6*, *17*). As a consequence, the phase function implemented by the metasurface can be relatively constant over a range of wavelengths. However, this is not sufficient to eliminate chromatic aberrations. In this Report, we demonstrate a new approach to planar optics based on metasurfaces that achieves achromatic behavior at multiple wavelengths and offers a potentially practical route to circumventing the limitations of both refractive and standard diffractive optics.

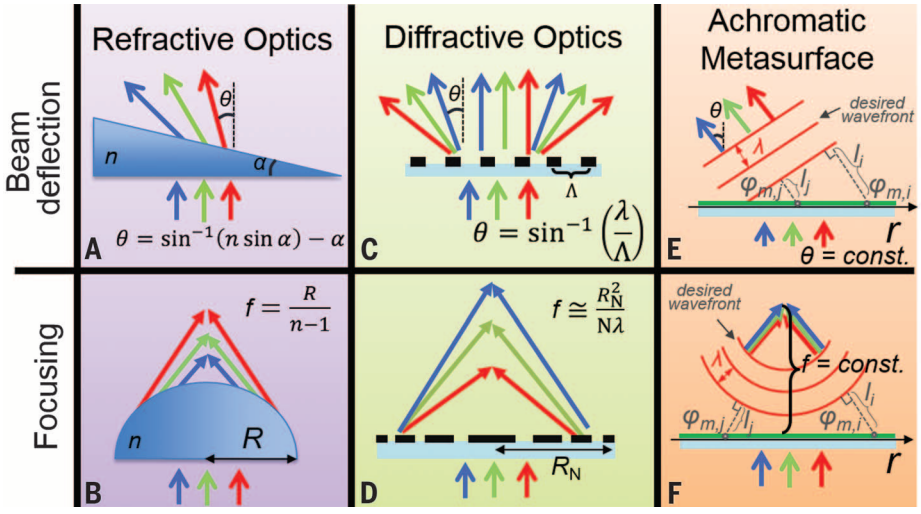

Fig. 1. Comparison between refractive optics, diffractive optics, and achromatic metasurfaces. In the first two cases (**A** to **D**), the angle of deflection θ and the focal length *f* change as a function of wavelength. The achromatic metasurface (**E** and **F**) consisting of subwavelength spaced resonators is designed to preserve its operation (same θ and *f*) for multiple wavelengths. To achieve this, the phase shifts $\varphi_{m,i}$ and $\varphi_{m,j}$ imparted by the metasurface at points r_i and r_j of the interface are designed so that the paths $l_i = l(r_i)$ and $l_j = l(r_j)$ are optically equivalent at different wavelengths. α, apex angle of the prism; *R*, radius of curvature of the refractive lens; Λ, period of the grating; R_N and N, radius and number of rings of the diffractive lens, respectively.

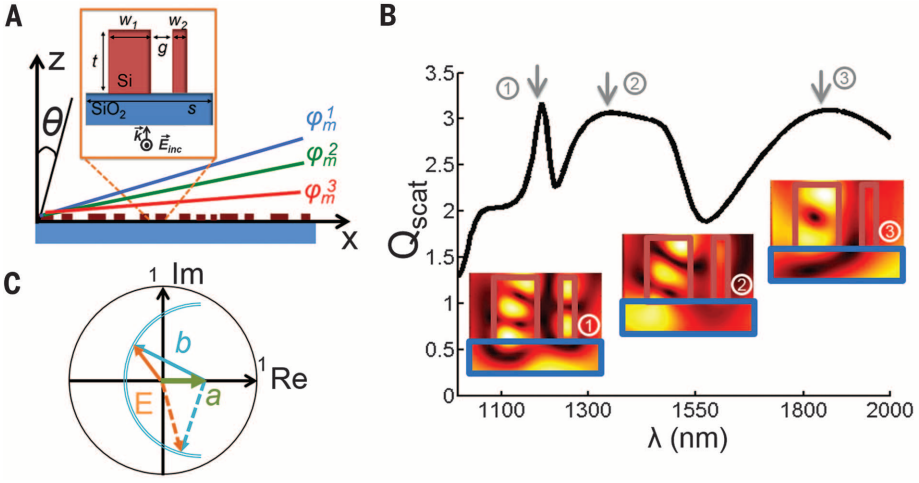

Fig. 2. Achromatic metasurface. (**A**) Side view of the metasurface made of 240 unit cells, each consisting of a slot of the same width *s*, comprising two coupled rectangular dielectric resonators of fixed height *t* and varying widths w_1 and w_2 (inset). The resonators are assumed to be 2D in the simulations because their length (240 μm) is much larger than the other dimensions. The metasurface is designed to diffract normally incident plane waves at three wavelengths (λ_1 = 1300 nm, λ_2 = 1550 nm, λ_3 = 1800 nm) by the same angle (θ_0 = –17°) by implementing a wavelength-dependent linear phase profile φ_m. $\vec{k}_\odot$ and $\vec{E}_{inc}$, incident wave vector and electric field, respectively. (**B**) Scattering efficiency Q_{scat} (defined as the ratio of the 2D scattering cross section, which has the dimension of a length, and the geometric length $w_1 + w_2$) for one unit cell with geometry *s* = 1 μm, *t* = 400 nm, w_1 = 300 nm, w_2 = 100 nm, and *g* = 175 nm. The spectrum has resonances due to the individual resonators (2 and 3) and to the coupling between the resonators (1), as shown by the electric field intensity ($|E|^2$) distributions. (**C**) Vector representation of the interference between the electric fields scattered by the slot and by the resonators, proportional to *a* and *b*, respectively. The vector sum of *a* (green) and *b* (blue) is represented by the phasor *E* (orange) for two different wavelengths (solid and dashed lines). Im, imaginary; Re, real.

Any desired functionality (focusing, beaming, etc.) requires constructive interference between multiple light paths separating the interface and the desired wavefront [i.e., same total accumulated phase φ_{tot} modulo 2π for all light paths (Fig. 1, E and F)]. The total accumulated phase is the sum of two contributions: $\varphi_{tot}(r,\lambda) = \varphi_m(r,\lambda) + \varphi_p(r,\lambda)$, where φ_m is the phase shift imparted at point *r* by the metasurface and φ_p is the phase accumulated via propagation through free space. The first term is characterized by a large variation across the resonance. The second is given by $\varphi_p(r,\lambda) = \frac{2\pi}{\lambda} l(r)$, where $l(r)$ is the physical distance between the interface at position *r* and the desired wavefront (Fig. 1, E and F). To ensure achromatic behavior of the device (e.g., deflection angle or focal length independent of wavelength), the condition of constructive interference should be preserved at different wavelengths by keeping φ_{tot} constant. The dispersion of φ_m has to be designed to compensate for the wavelength dependence of φ_p

$$\varphi_m(r,\lambda) = -\frac{2\pi}{\lambda} l(r) \qquad (1)$$

where $l(r)$ contains information on the device function [i.e., beam deflector (*5*, *6*), lens, axicon (*12*), etc.]. Equation 1 is the cornerstone for the design of an achromatic metasurface. This approach to flat optics features the advantages of diffractive optics, such as flatness and small footprint, while achieving achromatic operation at selected design wavelengths (Fig. 1). As an example of an achromatic metasurface, we demonstrate a beam deflector based on dielectric resonators: Whereas the typical function of a diffractive grating is the angular separation of different wavelengths, we show beam deflection with a wavelength-independent angle of deflection θ for three discrete telecom wavelengths.

The basic unit of the achromatic multiwavelength metasurface is a subwavelength-size resonator designed to adjust the scattering phase shift at different wavelengths $\varphi_m(r,\lambda)$ to satisfy Eq. 1. In this work, coupled rectangular dielectric resonators (RDRs) are used as building blocks

(*18*). Figure 2A shows the side view of the metasurface: A 240-μm-wide collection of 240-μm-long silicon (Si) RDRs patterned on a fused silica (SiO_2) substrate is designed to deflect normally incident light at an angle $\theta_0 = -17°$ for three different wavelengths (λ_1 = 1300 nm, λ_2 = 1550 nm, λ_3 = 1800 nm). The target spatially varying phase functions (Fig. 2A) are defined by (where x is the spatial coordinate of the metasurface)

$$\varphi_m(x, \lambda_i) = -\frac{2\pi}{\lambda_i}\sin\theta_0 x \text{ for } i = 1, 2, 3 \quad (2)$$

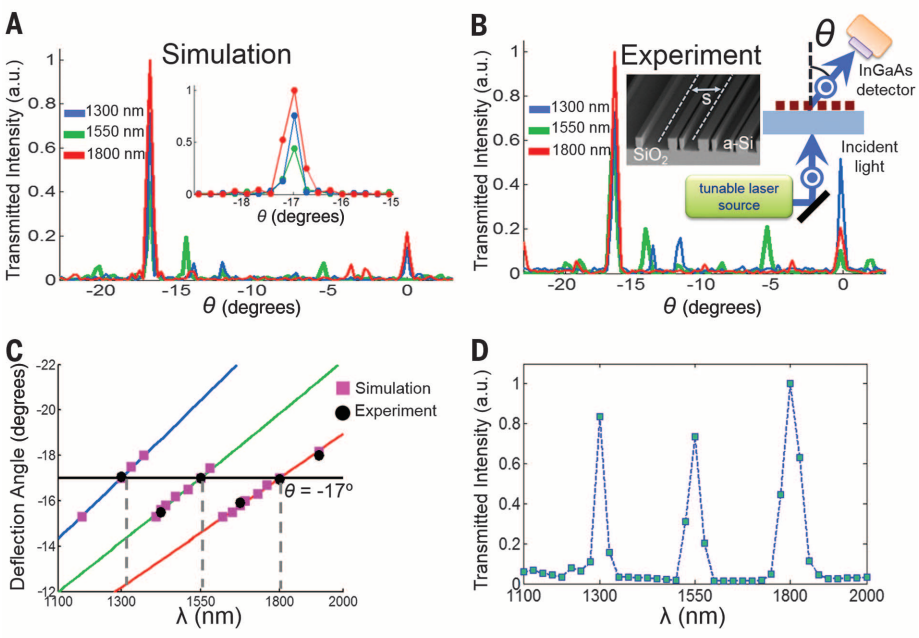

Fig. 3. Dispersion-free beam deflector. (**A**) Simulated far-field intensity (normalized to the maximum value for each of the three wavelengths) as a function of the angle θ from the normal to the interface. a.u., arbitrary units. (Inset) Zoomed-in view around the angle $\theta_0 = -17°$. (**B**) Far-field transmission measurements. (Insets) Schematic of the experimental setup and scanning electron microscopy image of a portion of the metasurface (s = 1 μm). (**C**) Measured (black circles) and simulated (pink squares) deflection angles for wavelengths from 1100 to 1950 nm. The colored lines are calculated from Eq. 2 for fixed phase gradients designed for $\theta_0 = -17°$ and λ =1300 nm (blue), 1550 nm (green), and 1800 nm (red), respectively. (**D**) Intensity measured by the detector at θ_0 as a function of wavelength.

The metasurface is divided into 240 subwavelength unit cells of equal width s, and for each section we choose two RDRs of fixed height t, varying widths w_1 and w_2, and separation g so that the phase response follows Eq. 2. Each unit cell, comprising a slot of width s with two RDRs (Fig. 2A), is different from the others, and therefore the metasurface is completely aperiodic, unlike other gradient metasurfaces (*5*, *11*) (fig. S7A).

Figure 2B shows the scattering cross section of an isolated unit cell excited with transverse-electric polarization. Given a plane wave traveling along the z axis and incident on the unit cell, at large distance from the interface ($\rho >> \lambda$) the field amplitude is given by two contributions: the light diffracted by the slot of width s and the field scattered by the coupled resonators (*19*, *20*)

$$E(\rho) \approx \frac{e^{jk\rho}}{\rho}[a + b(\theta)] \quad (3)$$

where j is the imaginary unit, k is the wave number of the light, a is the diffraction amplitude assuming the absence of the resonators and is in phase with the incident light, θ is the angle between ρ and the z axis, and $b(\theta)$ is the complex scattering function. Equation 3 is valid when the slot size s is much smaller than the free-space wavelength λ. This is not entirely applicable for our feature size; however, this approximation is sufficient to demonstrate the concept. The interference described by Eq. 3 makes it possible to adjust the phase values at several wavelengths simultaneously within a large range. This effect can be visualized using the complex field (phasors) representation in Fig. 2C. Whereas a is in phase with the incident field, the phase of b—associated with the scattered light due to the resonances of the dielectric resonators—spans the range ($\pi/2$, $3\pi/2$) (*11*, *21*). The vector sum E

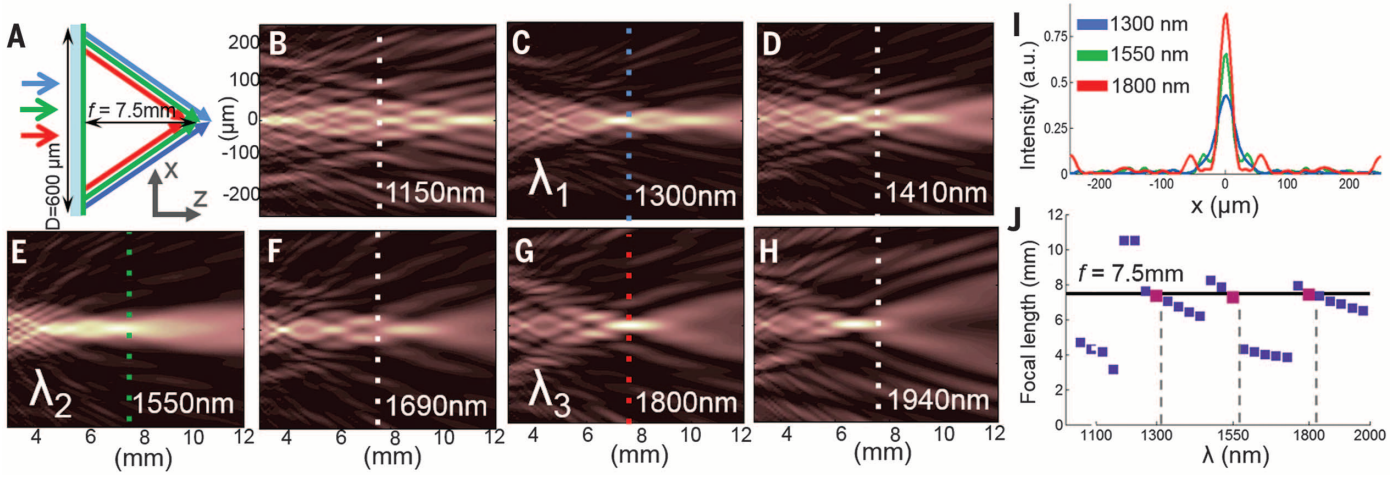

Fig. 4. Performance of a simulated achromatic flat lens. (**A**) A broadband plane wave illuminates the backside of the lens with side D = 600 μm and focal distance f = 7.5 mm. (**B** to **H**) Far-field intensity distribution for different wavelengths. The dashed lines correspond to the desired focal planes. (**I**) Cross section across the focal plane for λ_1, λ_2, and λ_3. (**J**) Focal lengths as a function of wavelength, calculated as the distance between the lens center and highest-intensity point on the optical axis. The three pink squares correspond to the wavelengths of interest.

can thus cover all four quadrants. Note that the scattering cross section Q_{scat} (Fig. 2B) used to visualize the resonance of the structure is related to the forward scattering amplitude $b(0)$ by the optical theorem (*20*).

Finite-difference time-domain (FDTD) simulations were performed to optimize the geometry of each unit cell to obtain the desired phase response $\varphi_m(x,\lambda)$ and approximately uniform transmitted amplitude for all unit cells at the three design wavelengths (*18*). We also simulated the entire structure and calculated the far-field distribution of light transmitted through the interface at several wavelengths. The fabrication procedure involving chemical vapor deposition of amorphous silicon, electron-beam lithography, and reactive ion etching, is described in the supplementary materials (*18*). Both the simulation and the experimental results show the multiwavelength achromatic behavior of the metasurface (Fig. 3): Whereas the dispersive nature of conventional flat and diffractive optical components would produce an angular separation of the three wavelengths, the angle of deflection at λ_1, λ_2, and λ_3 is the same ($\theta = -17°$). The diffraction order at the opposite side ($-\theta_0$) is completely suppressed (fig. S7), confirming that the structure does not present any periodicity and that the steering effect is the result of the phase gradient introduced by the subwavelength resonators. Simulations for different angles of incidence are presented in fig. S8. Figure 3C shows the simulated and measured deflection angles for normal incidence in the entire spectral range from 1150 to 1950 nm. As expected from the modeling, the device deflects the incident light by an angle θ_0 only for the designed wavelengths. The three colored lines in Fig. 3C are the theoretical angular dispersion curves obtained from Eq. 2 for metasurfaces designed for fixed wavelengths λ_1, λ_2, and λ_3. The overlap of the experimental and simulated data with these curves indicates that wavelengths other than λ_1, λ_2, and λ_3 tend to follow the dispersion curve of the closest designed wavelengths. Based on the same type of resonators with identical number of degrees of freedom (w_1, w_2, and g), we also designed four other metasurfaces with one, two, four, and five corrected wavelengths, respectively; each metasurface deflects the design wavelengths by the same angle, $\theta_0 = -17°$ (fig. S9). These results show that our design is wavelength scalable, paving the way for the creation of broadband metasurfaces that are able to suppress chromatic aberrations for a large number of wavelengths, using a reduced number of components compared with achromatic refractive optics (*3*, *4*). An important requirement for an achromatic optical device is uniform efficiency within the bandwidth (*1*). We measured the intensity at the angular position $\theta = -17°$ as a function of wavelength from 1100 to 2000 nm (Fig. 3D) and observed intensity variations of less than 13% at λ_1, λ_2, and λ_3 and large suppression ratios with respect to the other wavelengths (50:1). These properties suggest that this device can be used as an optical filter with multiple pass-bands [the full width at half maximum for each band is ~30 nm (fig. S10)]. The measured absolute efficiency of the device (power at θ_0 divided by the incident power) for the three wavelengths is 9.8%, 10.3%, and 12.6% for λ_1, λ_2, and λ_3, respectively. From the analysis of the FDTD simulations, we can understand the origin of the limited efficiency and how it can be improved (*18*).

The design of a flat lens based on RDRs for the same three wavelengths is also presented. This device is functionally equivalent to the bulk refractive lens known as apochromatic triplet or apochromat (*3*). The parameters s and t are the same as in the previous demonstration, and the values of w_1, w_2, and g for 600 unit cells are chosen so that the target phase functions are (*12*)

$$\varphi_m(x,\lambda_i) = -\frac{2\pi}{\lambda_i}\left(\sqrt{x^2+f^2}-f\right) \text{ for } i = 1,2,3 \quad (4)$$

where the focal distance f = 7.5 mm. Because we are using two-dimensional (2D) RDRs, the hyperbolic phase gradient is applied only in one dimension, imitating a cylindrical lens. The multiwavelength properties of the lens are demonstrated with FDTD simulations (Fig. 4). As expected, we observe good focusing at f = 7.5 mm for λ_1, λ_2, and λ_3 (Fig. 4, C, E, and G) and focusing with aberrations at other wavelengths (Fig. 4, B, D, F, and H). The diameters of the Airy disks at the focal spots are 50, 66, and 59 μm for λ_1, λ_2, and λ_3, respectively, achieving focusing close to the diffraction limit (40, 47, 55 μm; numerical aperture = 0.05) (Fig. 4I). For the wavelengths close to λ_1, λ_2, and λ_3, the focal distance follows the dispersion curve associated with the closest corrected wavelength (Fig. 4J). Recently, it was pointed out that to achieve broadband focusing, the phase shift distribution of a metasurface should satisfy a wavelength-dependent function, though a general approach to overcome this inherent dispersive effect was not provided (*22*).

In general, the phase function is defined up to an arbitrary additive constant. Therefore, Eq. 1 can be generalized as

$$\varphi_m(r,\lambda) = -\frac{2\pi}{\lambda}l(r) + C(\lambda) \quad (5)$$

For linear optics applications, the quantity $C(\lambda)$ can take on any value and thus can be used as a free parameter in the optimization of the metasurface elements. More generally, $C(\lambda)$ can be a relevant design variable in the regime of nonlinear optics, where the interaction between light of different wavelengths becomes important.

Metasurfaces have potential as flat, thin, and lightweight optical components that can combine several functionalities into a single device, making them good candidates to augment conventional refractive or diffractive optics (*5*–*8*). The multiwavelength metasurfaces demonstrated here circumvent one of the most critical limitations of planar optical components: the strong wavelength dependence of their operation (focusing, deflection, etc.). These devices could find application in digital cameras and holographic 3D displays, in which a red-green-blue filter is used to create a color image. Multiwavelength achromatic metasurfaces could also be implemented in compact and integrated devices for nonlinear processes. Our metasurface design is scalable from the ultraviolet to the terahertz and beyond and can be realized with conventional fabrication processes. Finally, the versatility in the choice of the wavelength-dependent phase allows for functionalities that are very different (even opposite) from the achromatic behavior discussed in this paper. For example, an optical device with enhanced dispersion (e.g., a grating able to separate different colors further apart) can be useful for ultracompact spectrometers.

REFERENCES AND NOTES

1. B. Kress, P. Meyrueis, *Applied Digital Optics* (Wiley, Hoboken, NJ, 2009).
2. E. Hecht, *Optics* (Addison Wesley, Boston, ed. 3, 1997).
3. F. L. Pedrotti, L. S. Pedrotti, *Introduction to Optics* (Prentice-Hall, Upper Saddle River, NJ, 1987).
4. R. Mercado, L. Ryzhikov, *Proc. SPIE* **3482**, 321–331 (1998).
5. N. Yu *et al*., *Science* **334**, 333–337 (2011).
6. N. Yu *et al*., *IEEE J. Sel. Top. Quantum Electron.* **19**, 4700423 (2013).
7. N. Yu, F. Capasso, *Nat. Mater.* **13**, 139–150 (2014).
8. A. V. Kildishev, A. Boltasseva, V. M. Shalaev, *Science* **339**, 1232009 (2013).
9. F. Aieta *et al*., *Nano Lett.* **12**, 1702–1706 (2012).
10. X. Ni, N. K. Emani, A. V. Kildishev, A. Boltasseva, V. M. Shalaev, *Science* **335**, 427 (2012).
11. D. Lin, P. Fan, E. Hasman, M. L. Brongersma, *Science* **345**, 298–302 (2014).
12. F. Aieta *et al*., *Nano Lett.* **12**, 4932–4936 (2012).
13. A. Pors, M. G. Nielsen, R. L. Eriksen, S. I. Bozhevolnyi, *Nano Lett.* **13**, 829–834 (2013).
14. S. Vo *et al*., *IEEE Photon. Technol. Lett.* **26**, 1375–1378 (2014).
15. W. T. Chen *et al*., *Nano Lett.* **14**, 225–230 (2014).
16. B. Yang, W. M. Ye, X. D. Yuan, Z. H. Zhu, C. Zeng, *Opt. Lett.* **38**, 679–681 (2013).
17. M. Kats *et al*., *Proc. Natl. Acad. Sci. U.S.A.* **109**, 12364–12368 (2012).
18. See supplementary materials on *Science* Online.
19. M. Born, E. Wolf, *Principles of Optics* (Cambridge Univ. Press, New York, ed. 7, 1999)
20. H. C. van de Hulst, *Light Scattering by Small Particles* (Dover, New York, 1981).
21. A. E. Krasnok, A. E. Miroshnichenko, P. A. Belov, Y. S. Kivshar, *Opt. Express* **20**, 20599–20604 (2012).
22. C. Saeidi, D. van der Weide, *Appl. Phys. Lett.* **105**, 053107 (2014).

ACKNOWLEDGMENTS

We acknowledge partial financial support from the Air Force Office of Scientific Research under grant FA9550-12-1-0389 (Multidisciplinary University Initiative), Draper Laboratory under program SC001-0000000731, and the NSF under program ECCS-1347251 (EAGER). We thank B. Kress (Google) for insightful remarks and suggestions; S. Kalchmair, R. Khorasaninejad, and J. P. Laine (Draper Laboratory) for helpful discussions; and E. Hu for the supercontinuum laser (NKT "SuperK"). The fabrication was performed at the Harvard Center for Nanoscale Systems, which is a member of the National Nanotechnology Infrastructure Network. The thin-film characterization of the amorphous silicon was done by Accurion.

SUPPLEMENTARY MATERIALS

www.sciencemag.org/content/347/6228/1342/suppl/DC1
Materials and Methods
Supplementary Text
Figs. S1 to S10
References (*23*–*29*)

14 November 2014; accepted 6 February 2015
Published online 19 February 2015;
10.1126/science.aaa2494

Multiwavelength achromatic metasurfaces by dispersive phase compensation

Francesco Aieta *et al.*

Science **347**, 1342 (2015);
DOI: 10.1126/science.aaa2494